THE JOURNAL OF PHYSICAL CHEMISTRY B

Article

pubs.acs.org/JPCB

Dissecting Structure of Prion Amyloid Fibrils by Hydrogen–Deuterium Exchange Ultraviolet Raman Spectroscopy

Victor Shashilov,[†] Ming Xu,[†] Natallia Makarava,[‡] Regina Savtchenko,[‡] Ilia V. Baskakov,[‡] and Igor K. Lednev*[,†]

[†]Department of Chemistry, University at Albany, SUNY, 1400 Washington Avenue, Albany, New York 12222, United States

[‡]Center for Biomedical Engineering and Technology and Department of Anatomy and Neurobiology, University of Maryland School of Medicine, Baltimore, Maryland 21201, United States

Supporting Information

ABSTRACT: The molecular mechanisms underlying structural diversity of amyloid fibrils or prion strains formed within the same primary structure is considered to be one of the most enigmatic questions in prion biology. We report here on the direct characterization of amyloid structures using a novel spectroscopic technique, hydrogen–deuterium exchange ultraviolet Raman spectroscopy. This method enables us to assess the structural differences within highly ordered cross-β-cores of two amyloid states produced within the same amino acid sequence of full-length mammalian prion protein. We found that while both amyloid states consisted of β-structures, their cross-β-cores exhibited hydrogen bonding of different strengths. Moreover, Raman spectroscopy revealed that both amyloid states displayed equally narrow crystalline-like bands, suggesting uniform structures of cross-β-cores within each state. Taken together, these data suggest that highly polymorphous fibrils can display highly uniform structures of their cross-β-core and belong to the same prion strain.

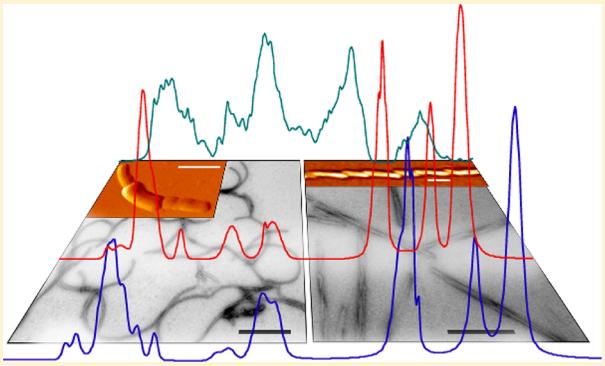

INTRODUCTION

Amyloid fibrils are associated with numerous debilitating maladies including Alzheimer's disease, Parkinson's disease, Huntington's diseases, and prion disease, etc.[1,2] The rational design of successful therapeutic strategies calls for detailed analysis of amyloid cross-β-sheet structures. Amyloid fibrils are noncrystalline and insoluble and, thus, are not amenable to conventional X-ray crystallography and solution NMR.[1] Wide-angle X-ray scattering[3] and transmission electron and scanning probe microscopies[1] have been routinely used for amyloid structure analysis. These methods, however, are insensitive to subtle differences in the Ψ and Φ torsional angles that define the conformation of the polypeptide backbone. Several specialized techniques have been recently developed for probing fibrillar structure.[3−10] X-ray diffraction can provide atomic-level insight into the β-strand assembly of microcrystals formed from short peptides (5−7 amino acid residues), thereby mimicking the core structure of fibrils formed from amyloidogenic proteins.[11−15] However, similar crystallographic data for full-length proteins are not yet feasible. Solid-state NMR (SSNMR) probes interatomic distances and torsion angles, which define local secondary structure and side-chain conformations.[5,16−18] This technique, however, requires site-specific ^{13}C and/or ^{15}N labels. Deep UV resonance Raman (DUVRR) spectroscopy is a powerful tool for protein structural characterization at all stages of fibrillation.[19−22] We have recently reported on the application of DUVRR spectroscopy combined with hydrogen–deuterium exchange (HX) for structural characterization of lysozyme fibril cross-β-core.[23,24] Here, we demonstrate the capacity of HX DUVRR spectroscopy for assessing the structure of two amyloid states produced from the same pool of highly pure full-length recombinant prion protein (PrP). Comparative characterization of two self-propagating amyloid states using DUVRR spectroscopy revealed differences in the strength of hydrogen bonding while showing a crystal type β-sheet structure for both fibril classes.

EXPERIMENTAL METHODS

Protein Expression. Syrian hamster full-length recombinant PrP encompassing residues 23−231 was expressed and purified as described earlier[25,26] with the following modifications. For the last step of purification conducted on a 25 mm × 25 cm C4 high-performance liquid chromatography (HPLC) column, the percentage of HPLC buffer B (0.1% trifluoracetic acid in acetonitrile) was increased from 0 to 25% during the first 15 min (at a flow rate of 5 mL/min). Then, a gentle gradient was applied (from 25 to 35% of buffer B in the next 65 min) to ensure efficient separation of PrP adducts. From there, the percentage of buffer B was increased from 35 to 100% in 15

Received: December 19, 2011
Revised: May 13, 2012
Published: June 8, 2012

min; the column was washed with 100% of buffer B for 15 min, and the gradient dropped down to 0% within 10 min. The correctly folded, oxidized, α-helical form of PrP was eluted as a major peak between 52.5 and 54.5 min. Minor amounts of truncated PrP polypeptides ($M_w \sim 21-22$ kDa, less than 1−2% of total PrP) were eluted in the tail of the major peak (elution time > 54.5 min). The fractions corresponding to the peak's tail were not used for the fibrillation reaction. The shoulder to the major peak containing PrP with oxidized methionines and eluted at <52.5 min was also discharged. Fractions eluted at 52.5−54.5 min were combined, lyophilized, and stored at −20 °C for not longer than 2 weeks prior to use. The purity of the final PrP was estimated by sodium dodecyl sulfate−polyacrylamide gel electrophoresis (SDS-PAGE) and electrospray mass spectroscopy to be >99.5%; the α-helical conformation was confirmed by CD (see Figure S1 in the Supporting Information).

Formation of S- and R-Fibrils. S- and R-fibrils were formed as previously described.[27] Briefly, PrP stock solution prepared in 5 mM HEPES, pH 7.0, was diluted with MES (pH 6.0) and 6 M GdnHCl to final concentrations of 50 mM and 2 M, respectively, and to a final protein concentration of 0.25 mg/mL. The S-fibrils were formed upon continuous shaking at 600 rpm using a Delfia plate shaker (Wallac) at 37 °C, whereas the R-fibrils were formed upon continuous rotation at 24 rpm using a Clay Adams Nutator (model 1105) at 37 °C. Both fibrillation reactions were completed within 48 h of incubation at 37 °C. The same, freshly prepared stock solution of PrP was used for the formation of both S- and R-fibrils.

SDS-PAGE in Denaturing and Nondenaturing Conditions. To estimate the yield of fibrillation, the aliquots were taken at the end points of the reactions and treated with two sample buffers: denaturing (the final 60 mM Tris, 2% SDS, and 1.25% β-mercaptoethanol, 2.25 M urea, heating for 15 min at 90 °C) and nondenaturing (no SDS, β-mercaptoethanol or urea, no heating). A 12% SDS-PAGE (precast NuPAGE gels, Invitrogen) was used for analysis of samples treated with both denaturing and nondenaturing sample buffers (Figure S2 in the Supporting Information).

DUVRR Measurements. A home-built DUVRR spectroscopic apparatus was described in detail elsewhere.[28,29] The 197 nm fourth harmonic generation of Indigo S laser system (Coherent, Inc.) was used for excitation. Raman scattering was dispersed and recorded using a home-built double monochromator coupled with a liquid nitrogen-cooled CCD camera (Roper Scientific, Inc.). A rotating Suprasil NMR tube with a magnetic stirrer inside was used as a sample holder. The acquired Raman spectra were analyzed using GRAMS/AI software (Thermo Electron Corp.). Spectral contributions of water and quartz were numerically subtracted. Sodium trifluoroacetate was used as the internal standard for intensity normalization. Raman spectra were calibrated relative to bands in Teflon spectra acquired before and after protein sample measurements. A relative variation in Teflon band positions was always within 0.5 cm^{-1} that determined the experimental accuracy of Raman peak position.

Spectrum Analysis/Interpretation. The Bayesian approach[30] was utilized for the mathematical separation of overlapping DUVRR bands of the deuterated unordered moieties and the protonated cross-β-core. The Bayesian source separation is a prior information-based approach and is typically used for solving spectral separation problems when there is enough prior information about the pure component spectra and their evolution profiles.

The Bayes theorem for the spectral separation problem takes the form:

$$P(C, S|\text{Data}, I) \sim P(\text{Data}|C, S, I)\cdot P(C|I)\cdot P(S|I) \quad (1)$$

where $P(\text{Data} \mid C,S,I)$ is the likelihood measuring the quality of data fitting and $P(S \mid I)$ and $P(C \mid I)$ are prior probabilities for individual component spectra and concentrations, respectively. The vertical bar "|" marks the conditional probability, with, for example, $P(\text{A} \mid \text{B})$ meaning the probability of A given B. Because finding either matrix C or S alone is enough for solving problem (1), the concentration matrix C is normally sought since it contains far fewer elements. In essence, the Bayesian theorem states that both the quality of data fitting $P(\text{Data} \mid C,S,I)$ and the physical meaning of the resolved spectral and concentration matrices $P(S \mid I)$ and $P(C \mid I)$ must be used as the criteria of the correctness of the multivariate model.[31]

The ultimate goal of this study was to separate Raman signatures of the fibril core and unordered parts from the set of DUVRR spectra acquired at various stages of HD exchange. The mathematical problem of isolating the fibril core spectrum could not be solved using any other conventional chemometrics methods because of the 100% correlation of the concentration profiles of contributing species. The ill conditioning of the problem was eliminated by incorporating prior information about the concentration matrix and the spectral features of the individual components into the Bayesian equation.

The data set consisted of DUVRR spectra of fibrils suspended in D_2O/H_2O mixture with a D_2O concentration ranging from 0 to 100% at 10% increments. The HD exchange method[22] exploits the fact that gradual substitution of H_2O with D_2O in an aqueous suspension of mature fibrils results in partial HD exchange in amide groups of polypeptide backbone segments accessible to the solvent, while the fibril core remains fully protonated. Amyloid fibrils are composed of the highly ordered β-sheet core surrounded by unordered fragments. The main chain NH group protons in proteins show facile exchange when exposed to the D_2O environment.[32] In the hydrophobic cross-β-core, which is hidden from the solvent, the rates of HD exchanges are strongly reduced. Hence, amide N−H protons in unordered fragments of amyloid fibrils should be readily exchanged, while those buried in the cross-β-structure will remain protonated. As a result, deuteration will cause Raman bands of β-turns and unordered parts of fibrils to shift and change their Raman cross-sections but will have no effect on the Raman signature of the cross-β-core.

To solve the source separation problem (1), all a priori information about characteristic bands in the individual component spectra (matrix S, see eq 1) was incorporated via the Bayesian signal dictionary approach[33] where individual components are presented as a linear combination of reference spectral bands. The concentration matrix (matrix C, see eq 1) was constrained to the fractions of protonated and deuterated species controlled in the experiment and to the fraction of the fibrillar core that was iteratively refined during the optimization by genetic algorithm.[34] The spectra of three pure components (cross-β-core, the protonated, and the deuterated unordered moieties) were sought using all prior information such as concentration profiles and spectral features of the pure components.[23]

dx.doi.org/10.1021/jp2122455 | J. Phys. Chem. B 2012, 116, 7926−7930

RESULT AND DISCUSSION

Two amyloid states referred to as S- and R-fibrils were prepared in vitro under identical solvent conditions but different shaking modes using the same pool of highly pure full-length Syrian hamster recombinant PrP (see the Supporting Information). As shown previously,[27,35] the S- and R-fibrils exhibited different morphologies as evident from electron microscopy (EM) and atomic force microscopy (AFM) (Figure 1), and different

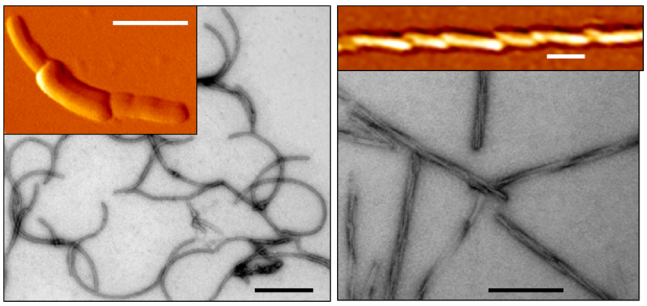

Figure 1. EM and AFM (insets) images of S-fibrils (left) and R-fibrils (right). Scale bars correspond to 0.2 μm.

folding patterns as probed by FTIR, CD, immunoconformational assays, Proteinase K-digestion assay, and X-ray diffraction analysis. Furthermore, the individual S- and R-specific conformations could be transferred to daughter fibrils in cross-seeding experiments conducted under alternative shaking modes.[27]

To analyze the structure of the cross-β-core, DUVRR spectra were recorded for both fibril states suspended in H_2O/D_2O mixtures with the D_2O fraction ranging from 0 to 100% at 10% increments (Figure 2). The DUVRR cross-β-core signatures were isolated using Bayesian statistics.[23]

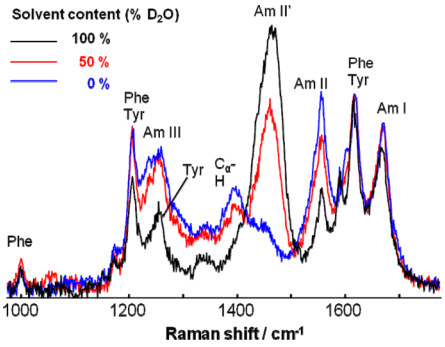

Figure 2. DUVRR spectra of S-fibrils in H_2O, D_2O/H_2O mixture, and 100% D_2O. The amide I mode (Am I) consists of carbonyl C=O stretching, with a small contribution from C–N stretching and N–H bending. Amide II and amide III bands involve significant C–N stretching, N–H bending, and C–C stretching. The C_α–H bending vibrational mode involves C_α–H symmetric bending and C–C_α stretching.[46]

HX caused the down-shift of the amide II DUVRR band from ~1555 to ~1450 cm^{-1} and virtual disappearance of the amide III band originating from unordered protein,[36] while DUVRR amide bands of the protonated cross-β-core remained unchanged[23] (Figure 2). The spectra were found to fit well to a linear combination of three components, that is, Raman spectra of (i) the protonated fibrillar cross-β-core, (ii) deuterated solvent-accessible part of fibrils predominantly in the unordered conformation, and (iii) the latter component in the protonated form, which were separated using the Bayesian approach. DUVRR spectra of cross-β-cores for both fibril types showed sharp amide I, amide II, C_α–H bending, and amide III bands centered around 1674, 1559, 1400, and 1220 cm^{-1}, respectively (Figure 3). Amide III bands were dominated by the ~1220 cm^{-1} band with small shoulders at 1227, 1235, and 1250 cm^{-1}. The major peak at ~1220 cm^{-1} derives from C–N stretching and N–H bending of anhydrous β-sheet, while the minor sub-bands at 1227, 1235, and 1250 cm^{-1} could correspond to the hydrated β-structure,[36] with the band frequency increasing with the degree of hydration. In addition, some β-turns not affected by deuteration can also contribute to the 1227 and 1250 cm^{-1} DUVRR bands. According to the Asher approach,[36] the average Ramachandran Ψ facial angle of the amide group can be calculated based on the spectral position of amide III DUVRR band. Using the equation for anhydrous β-sheet structure[36]

$$\nu^{\beta}_{\mathrm{AmIII}}(\Psi) = 1239\ \mathrm{cm}^{-1} - 54\ \mathrm{cm}^{-1}\cdot\sin(\Psi + 26^\circ) \qquad (2)$$

the corresponding DUVRR peak at 1220 cm^{-1} gave the value of the amide group facial angle of about 135° for both fibril types. As a reference, we collected the DUVRR spectra of globular β2-microglobulin (β2M) known to consist of seven β-strands organized into two antiparallel β-sheets.[37] Amide III band at ~1220 cm^{-1} in the DUVRR spectrum of β2M could be attributed tentatively to the anhydrous β-sheet.[36] The higher intensity of sub-bands at 1227, 1235, and 1250 cm^{-1} in the DUVRR spectrum of β2M relative to the amide III band of PrP fibrils is indicative of more extensive hydration of β-structure in the globular protein than in fibrillar cross-β-core (Figure 3). The position of A and B_2 bands (amide I mode, Figure 3, inset) is consistent with β-sheet structure in both types of PrP fibrils. The presence of the low-wavenumber B_2 Raman band reflects a pleated β-sheet with D_{2h} symmetry.[38]

Detailed analysis of DUVRR spectra revealed that amide I sub-bands of S-fibrils are upshifted, while the amide II band is downshifted relative to the corresponding bands in R-fibrils (Figure 3, inset). Noteworthy here is that these shifts were obvious for the experimental Raman spectra of fibril solutions (not shown) and were reproduced in the spectra of the fibril core obtained using the Bayesian approach (Figure 3, inset). These shifts are consistent with the stronger hydrogen-bonding interaction in cross-β-core of R-fibrils.[39] This change in hydrogen bonding can arise from different interstrand interactions in various classes of steric zippers as evident from different interstrand spacing in those structures.[14] Although the DUVRR cross-β-core signature clearly indicates a certain structural difference between the S- and the R-fibrils, more precise structural interpretation would require better understanding of the spectrum–structure relationship.

The first three examples of cross-β-core Raman signatures, those obtained for PrP fibrils here, synthetic polypeptide fibrils[21] and lysozyme fibrils,[23] indicated very ordered, crystalline-like structures. No inhomogeneous broadening by diverse amino acids was evident; yet, the cross-β-core Raman spectroscopic signature was different for all three fibrillar samples. Furthermore, clear differences in the Raman spectra of S- and R-fibrils indicated structural variations in fibrils formed within the same amino acid sequence using the same pool of highly pure recombinant PrP. While comprehensive interpretation of these differences requires better understanding of the spectrum–structure relationship, the present studies revealed that R-fibrils exhibited stronger hydrogen bonding than S-

dx.doi.org/10.1021/jp2122455 | J. Phys. Chem. B 2012, 116, 7926–7930

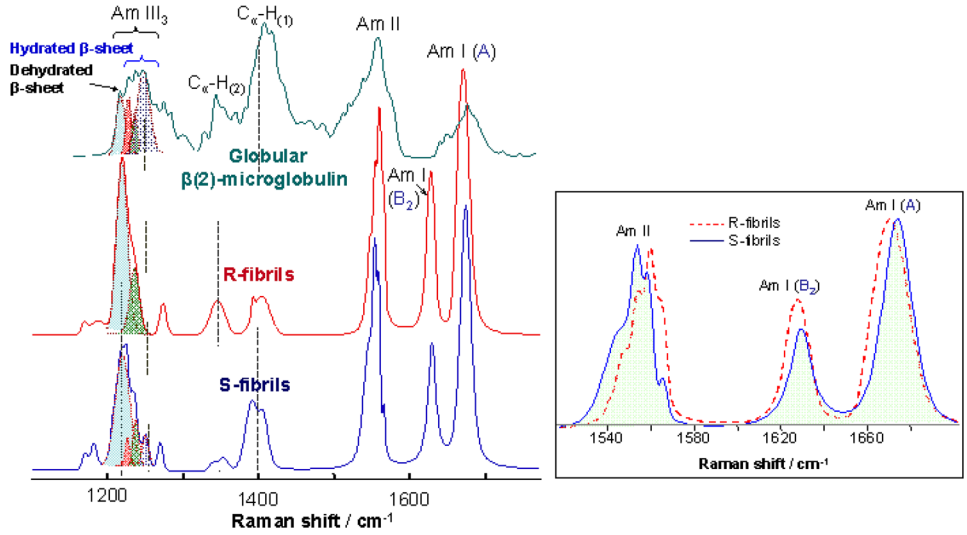

Figure 3. DUVRR spectra of antiparallel β-sheet-rich globular β2M and cross-β-core of R-fibrils (red) and S-fibrils (blue). The cross-β-core spectra were extracted from the data sets obtained for partially deuterated fibrils using a Bayesian approach.[23] Inset: Amide I and amide II region of R- and S-fibril Raman spectra.

fibrils. Notable, our recent studies demonstrated that R-fibrils were able to trigger transmissible prion disease in wild-type animals, whereas S-fibrils did not.[40] Further studies using a variety of structural techniques will help to identify molecular features responsible for prion infectivity.

Understanding the structural basis of prion strains is considered to be one of the most urgent problems in prion biology.[41] What level of assembly of highly ordered self-propagating states accounts for diversity of prion strains and amyloid structures?[42] The strain-specific variations might be encoded at the level of quaternary structure, in different modes of lateral association of protofilaments, or in protofilament substructure including the hydrogen-bonding networks and side-chain packing.[42] It is evident from the results presented here that although the type of β-strand conformation in the fibril core was very similar for S- and R-fibrils, there was a noticeable difference in the hydrogen bond strength, indicating a difference in the fibril core atomic structure of these two amyloid states. This subtle difference in atomic structure might give rise to differences in observed fibril morphologies. The results obtained by Raman spectroscopy were consistent with our previous findings where R- and S-amyloid states were found to display a significantly different folding pattern of the PrP polypeptide chain within the cross-β-spine.[35]

As judged from EM and AFM imaging, R- and S-fibrils exhibited substantially different degrees of polymorphism, where R-fibrils were much more diverse morphologically than S-fibrils.[27,43] The DUVRR spectra, however, displayed equally narrow crystalline-like bands for both types of fibrils, revealing that both S and R types have uniform conformations within their cross-β-cores. Taken together, these findings illustrate that structurally uniform, individual cross-β-cores can produce either morphologically diverse or relatively homogeneous populations of fibrils (Figure 4). This finding has several important implications. First, our study indicates that the relationship between fibril morphology and strain-specific structural features might be complex and that individual fibril morphology should not be considered as a signature of individual strain-specific structures. Second, it predicts that highly polymorphous fibrils could display a uniform structure and belong to the same

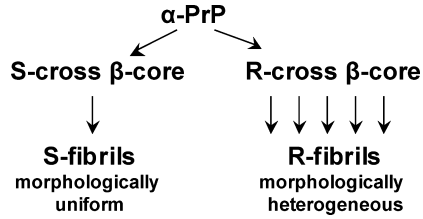

Figure 4. DUVRR spectroscopy revealed uniform conformation of cross-β-cores for both R- and S-fibrils. Structurally uniform, individual cross-β-cores, however, can produce either morphologically diverse (R-fibrils) or relatively homogeneous (S-fibrils) population of fibrils.

amyloid or prion strain. Indeed, scrapie fibrils derived from animals infected with different prion strains were found to display high levels of polymorphism within each individual strain.[44,45]

DUVRR spectroscopy is a novel method for acquiring quantitative information on peptide backbone conformation. When combined with HX, DUVRR spectroscopy can determine the Ramachandran Ψ angle in cross-β-structures of fibrils produced from large polypeptides such as full-length PrP.[23] Our current knowledge about fibril structure has been attributed largely to advances in SSNMR[5,16,17] and the recent successes in growing microcrystals.[11−15] SSNMR, however, requires site-specific ^{13}C and/or ^{15}N labeling, while atomic resolution X-ray is limited to small peptides. EPR spectroscopy offers an alternative approach for probing the structure of fibrils; however, this method requires production and spin labeling of multiple site-directed Cys variants. The HD-DUVRR method described here does not require isotope labeling and opens new opportunities for comparative study of fibrils prepared from large globular proteins that are not suitable for X-ray crystallography. We also envision using this technique for structural comparison of fibrils formed in vivo and in vitro.

■ ASSOCIATED CONTENT

Supporting Information

Figures S1 and S2. This material is available free of charge via the Internet at http://pubs.acs.org.

dx.doi.org/10.1021/jp2122455 | J. Phys. Chem. B 2012, 116, 7926−7930

AUTHOR INFORMATION

Corresponding Author

*E-mail: ilednev@albany.edu.

Notes

The content is solely the responsibility of the authors and does not necessarily represent the official views of the National Institutes of Health.

The authors declare no competing financial interest.

ACKNOWLEDGMENTS

This project is supported by Award Number R01AG033719 from National Institute on Aging, National Institutes of Health (I.K.L.), and Award Number NS045585 (I.V.B.).

REFERENCES

(1) Chiti, F.; Dobson, C. M. *Annu. Rev. Biochem.* **2006**, *75*, 333−366.

(2) Kelly, J. W. *Curr. Opin. Struct. Biol.* **1998**, *8*, 101−106.

(3) Squires, A. M.; Devlin, G. L.; Gras, S. L.; Tickler, A. K.; MacPhee, C. E.; Dobson, C. M. *J. Am. Chem. Soc.* **2006**, *128*, 11738−11739.

(4) Ma, S.; Cao, X.; Mak, M.; Sadik, A.; Walkner, C.; Freedman, T. B.; Lednev, I. K.; Dukor, R. K.; Nafie, L. A. *J. Am. Chem. Soc.* **2007**, *129*, 12364−12365.

(5) Tycko, R. *Q. Rev. Biophys.* **2006**, 1−55.

(6) Frare, E.; Mossuto, M. F.; Laureto, P. P. d.; Dumoulin, M.; Dobson, C. M.; Fontana, A. *J. Mol. Biol.* **2006**, *361*, 551−561.

(7) Mastrangelo, I. A.; Ahmed, M.; Sato, T.; Liu, W.; Wang, C.; Hough, P.; Smith, S. O. *J. Mol. Biol.* **2006**, *358*, 106−119.

(8) Adachi, R.; Yamaguchi, K.; Yagi, H.; Sakurai, K.; Naiki, H.; Goto, Y. *J. Biol. Chem.* **2007**, *282*, 8978−8983.

(9) Petty, S. A.; Decatur, S. M. *J. Am. Chem. Soc.* **2005**, *127*, 13488−13489.

(10) Cobb, N. J.; Sonnichsen, F. D.; McHaourab, H.; Surewicz, W. K. *Proc. Natl. Acad. Sci. U.S.A.* **2007**, *104*, 18946−18951.

(11) Eisenberg, D.; Nelson, R.; Sawaya, M. R.; Balbirnie, M.; Sambashivan, S.; Ivanova, M. I.; Madsen, A. O.; Riekel, C. *Acc. Chem. Res.* **2006**, *39*, 568−575.

(12) Nelson, R.; Eisenberg, D. *Curr. Opin. Struct. Biol.* **2006**, *16*, 260−265.

(13) Nelson, R.; Sawaya, M. R.; Balbirnie, M.; Madsen, A. O.; Riekel, C.; Grothe, R.; Eisenberg, D. *Nature* **2005**, *435*, 773−778.

(14) Sawaya, M. R.; Sambashivan, S.; Nelson, R.; Ivanova, M. I.; Sievers, S. A.; Apostol, M. I.; Thompson, M. J.; Balbirnie, M.; Wiltzius, J. J. W.; McFarlane, H. T.; Madsen, A. Ø.; Riekel, C.; Eisenberg, D. *Nature* **2007**, *447*, 453−457.

(15) Inouye, H.; Sharma, D.; Goux, W. J.; Kirschner, D. A. *Biophys. J.* **2006**, *90*, 1774−1789.

(16) van der Wel, P. C.; Lewandowski, J. R.; Griffin, R. G. *J. Am. Chem. Soc.* **2007**, *129*, 5117−5130.

(17) Jaroniec, C. P.; MacPhee, C. E.; Astrof, N. S.; Dobson, C. M.; Griffin, R. G. *Proc. Natl. Acad. Sci. U.S.A.* **2002**, *99*, 16748−16753.

(18) Tycko, R.; Savtchenko, R.; Ostapchenko, V. G.; Makarava, N.; Baskakov, I. V. *Biochemistry* **2010**, *49*, 9488−9497.

(19) Shashilov, V.; Xu, M.; Ermolenkov, V. V.; Fredriksen, L.; Lednev, I. K. *J. Am. Chem. Soc.* **2007**, *129*, 6972−6973.

(20) Shashilov, V. A.; Lednev, I. K. *J. Am. Chem. Soc.* **2008**, *130*, 309−317.

(21) Sikirzhytski, V.; Topilina, N. I.; Higashiya, S.; Welch, J. T.; Lednev, I. K. *J. Am. Chem. Soc.* **2008**, *130*, 5852−5853.

(22) Shashilov, V. A.; Sikirzhytski, V.; Popova, L. A.; Lednev, I. K. *Methods* **2010**, *52*, 23−37.

(23) Xu, M.; Shashilov, V.; Lednev, I. K. *J. Am. Chem. Soc.* **2007**, *129*, 11002−11003.

(24) Popova, L. A.; Kodali, R.; Wetzel, R.; Lednev, I. K. *J. Am. Chem. Soc.* **2010**, *132*, 6324−6328.

(25) Bocharova, O. V.; Breydo, L.; Parfenov, A. S.; Salnikov, V. V.; Baskakov, I. V. *J. Mol. Biol.* **2005**, *346*, 645−659.

(26) Breydo, L.; Bocharova, O. V.; Makarava, N.; Salnikov, V. V.; Anderson, M.; Baskakov, I. V. *Biochemistry* **2005**, *44*, 15534−15543.

(27) Makarava, N.; Baskakov, I. V. *J. Biol. Chem.* **2008**, *283*, 15988−15996.

(28) Lednev, I. K. Protein Structures. In *Methods in Protein Structures and Stability Analysis*; Uversky, V. N., Permyakov, E. A., Eds.; Nova Science Publishers, Inc.: New York, 2007.

(29) Lednev, I. K.; Ermolenkov, V. V.; He, W.; Xu, M. *Anal. Bioanal. Chem.* **2005**, *381*, 431−437.

(30) Knuth, K. *SPIE'98 Proceedings: Bayesian Inference for Inverse Problems*; SPIE: San Diego, July, 1998; Vol. *3449*, pp 147−158.

(31) Sivia, D. S.; Skilling, J. *Data Analysis: A Bayesian Tutorial*, 2nd ed.; Oxford University Press: Oxford, New York, 2006.

(32) Englander, S. W.; Sosnick, T. R.; Englander, J. J.; Mayne, L. *Curr. Opin. Struct. Biol.* **1996**, *6*, 18−23.

(33) Zibulevsky, M.; Pearlmutter, B. A. *Neural Comput.* **2001**, *13*, 863−882.

(34) Goldberg, D. *Genetic Algorithms in Search, Optimization, and Machine Learning*: Addison Wesley: Reading, MA, 1989.

(35) Ostapchenko, V. G.; Sawaya, M. R.; Makarava, N.; Savtchenko, R.; Nilsson, K. P.; Eisenberg, D.; Baskakov, I. V. *J. Mol. Biol.* **2010**, *400*, 908−921.

(36) Mikhonin, A. V.; Bykov, S. V.; Myshakina, N. S.; Asher, S. A. *J. Phys. Chem. B* **2006**, *110*, 1928−1943.

(37) Radford, S. E.; Gosal, W. S.; Platt, G. W. *Biochim. Biophys. Acta, Proteins Proteomics* **2005**, *1753*, 51−63.

(38) Yu, N.-T.; Krimm, S. *CRC Crit. Rev. Biochem.* **1977**, *4*, 229−280.

(39) Asher, S. A.; Mikhonin, A. V.; Bykov, S. *J. Am. Chem. Soc.* **2004**, *126*, 8433−8440.

(40) Makarava, N.; Kovacs, G. G.; Bocharova, O.; Savtchenko, R.; Alexeeva, I.; Budka, H.; Rohwer, R. G.; Baskakov, I. V. *Acta Neuropathol.* **2010**, *119*, 177−187.

(41) Krishnan, R.; Lindquist, S. L. *Nature* **2005**, *435*, 765−772.

(42) Kodali, R.; Wetzel, R. *Curr. Opin. Struct. Biol.* **2007**, *17*, 48−57.

(43) Anderson, M.; Bocharova, O. V.; Makarava, N.; Breydo, L.; Salnikov, V. V.; Baskakov, I. V. *J. Mol. Biol.* **2006**, *358*, 580−596.

(44) Sim, V. L.; Caughey, B. *Neurobiol. Aging* **2008**.

(45) Liberski, P. P.; Brown, P.; Xiao, S. Y.; Gajdusek, D. C. *J. Comp. Pathol.* **1991**, *105*, 377−386.

(46) Chi, Z.; Chen, X. G.; Holtz, J. S.; Asher, S. A. *Biochemistry* **1998**, *37*, 2854−2864.